JOURNAL OF PROPULSION AND POWER
Vol. 20, No. 6, November–December 2004

Using Aluminum for Space Propulsion

Antonella Ingenito* and Claudio Bruno†
University of Rome "La Sapienza," 00185 Rome, Italy

The combination of aluminum and water was theoretically analyzed to assess its performance potential for space propulsion, in particular for microrocket applications and whenever a compact package is desirable. Heat of reaction, impulse density, and handling safety are features making this combination interesting for chemical thrusters, especially because thrust is higher than typical of satellite electric thrusters. Ideal specific impulse I_{sp}, thrust coefficient, adiabatic flame temperature, and combustion products were calculated for chamber pressures 1–10 atm, nozzle area ratios 25–100, and mixture ratios O/F 0.4–8.0. I_{sp} reaches up to 3500 m/s. Also, the effect of hydrogen peroxide addition to aluminum and water on performance was explored. This combination improves performance slightly at the expense of simplicity, making it less attractive for microrocket engines. Ignition delay times were conservatively estimated assuming that aluminum was coated with its oxide and ignition occurred after the melting of the aluminum oxide. For this purpose heating and kinetics times were evaluated, the first by a one-dimensional physical model, the second by a reduced scheme. Results indicate that the heating time of a 0.1-μm-diameter aluminum particle may be of order 0.4 μs, whereas overall kinetics takes 10 μs: thus, the Al/water combination looks practical in principle for microrocket chambers characterized by short residence times.

Introduction

ALUMINUM and water have been proposed as propellants both for space[1] and for underwater propulsion,[2,3] where seawater plays the same role as freely available air in airbreathing engines. This propellant combination, as well as its products, is nontoxic and can be called "green." Interest in it was also recently spurred by the commercial availability of Al nanoparticles (ALEX^{TM})[4] and by reports of their successful use in liquid hydrocarbons/air combustion, where their high specific surface area would suggest rapid burn times. The combustion of an aluminum 'grain' or porous sponge with steam could form the basis for an alternative hybrid rocket motor; steam production could be integral to the regenerative cooling system, that is, produced from water by heat transfer from the combustion chamber. Last, a remarkable option is to burn pure Al with water, bypassing the heating and melting problems posed by its oxide. This is made possible by specialized manufacturing, resulting in a hypergolic hybrid motor.

Thermodynamically, this propellant combination is interesting because of its high heat of reaction. Pure (bare) Al reacts exothermically with oxygen, following the global reaction

$$2\mathrm{Al(s)} + 3/2\mathrm{O_2(g)} \leftrightarrow \mathrm{Al_2O_3(s)}$$

$$[\Delta H_{R^\circ}(298\ \mathrm{K}) = -404\ \mathrm{kcal/mol}] \qquad (1)$$

In an oxygen environment, Al is rapidly coated by a layer of alumina (Al_2O_3). In fact, Friedman and Macek[5] assume that aluminum reactions are frozen at temperatures below the melting temperature of Al_2O_3 (2327 K at $P = 1$ atm). If so, ignition is then controlled by the heating and melting of the Al_2O_3 layer and by Al–O_2 surface oxidation kinetics.

Once ignition occurs whether or not Al burns heterogeneously depends on the so-called Glassman criterion (see Refs. 6–8). In its final form[6] this criterion states that a metal burns in the vapor phase if its boiling temperature (2792.15 K for Al at 1 atm) is lower than the volatilization temperature of its oxide. In fact, for a liquid or solid fuel to burn as a vapor, its flame temperature must be higher than its fuel saturation temperature, so that it can vaporize, diffuse toward the oxidizing atmosphere, and react.[6] Thus, were pure Al vapor to burn with O_2, the adiabatic flame temperature would be much higher than the Al_2O_3 boiling point and correspond to the volatilization temperature (of order 3500 K at $P = 1$ atm). Actually, the flame temperature of an oxide-coated Al particle has instead an upper limit, that is, the boiling temperature of the oxide, because the boiling enthalpy of Al_2O_3 is greater than that available, that is, the reaction enthalpy of Al [$\Delta H_{R^\circ}(298\ \mathrm{K}) = -404$ kcal/mol for Al/O_2] minus the enthalpy required to heat Al_2O_3 above its boiling point (Table 1).

So, according to Ref. 6, ignition of an oxide-coated Al particle occurs only after the Al_2O_3 layer melts. Lowering the ignition temperature of Al is possible in principle by oxidizing Al with steam following the reaction $\mathrm{Al(s)} + 2\mathrm{H_2O} = \mathrm{AlOH(s)} + 3/2\mathrm{H_2}$: thus, in a steam atmosphere, Al particles are covered by a less protective hydroxide layer, requiring ignition temperatures in the range 1600–1700 K, and shortening ignition delay.[9] Oxidizing AlOH with water follows the reaction $2\mathrm{AlOH} + \mathrm{H_2O} = \mathrm{Al_2O_3(s)} + 2\mathrm{H_2}$. Summing the two reactions, one obtains

$$2\mathrm{Al(s)} + 3\mathrm{H_2O(g)} \leftrightarrow \mathrm{Al_2O_3(s)} + 3\mathrm{H_2}$$

$$[\Delta H_{R^\circ}(298\mathrm{K}) = -230\ \mathrm{kcal/mol}] \qquad (2)$$

Gurevich (see Ref. 10) found that the ignition temperature of (2) was considerably lower than the Al_2O_3 melting point, depending on the crystal structure of the AlOH oxide film initially covering the surface of aluminum. The energy release of Al and water, reaction (2), is about half of that of reaction (1). It is possible, in principle, to burn H_2 produced by (2) with additional (stored) O_2:

$$3\mathrm{H_2(s)} + 3/2\mathrm{O_2(g)} \leftrightarrow 3\mathrm{H_2O(g)}$$

$$[\Delta H_{R^\circ}(298\ \mathrm{K}) = -174\ \mathrm{kcal/mol}] \qquad (3)$$

In other words, following reactions (2) and (3), it is possible to obtain reaction (1) and the same energy release, but with less demanding ignition requirements. Reaction (3) does not need an external ignition source because H_2 produced in reaction (2) will be above its temperature of autoignition with O_2. On the other hand, in a space

Received 10 September 2003; revision received 21 April 2004; accepted for publication 29 April 2004.

*Ph.D. Student, Department of Mechanics and Aeronautics, Via Eudossiana 18; antonella.ingenito@uniroma1.it.

†Professor, Department of Mechanics and Aeronautics, Via Eudossiana 18; claudio.bruno@uniroma1.it. Fellow AIAA.

Table 1 Characteristic standard temperatures and energies of aluminum and alumina

Parameter	Aluminum	Alumina
Melting temperature	933.52 K	2327 K
Boiling temperature	2792.15 K	3273 K
Volatilization temperature	——	3450–4000 K
Melting heat	2.57 kcal/mol$_{Al}$	28.29 kcal/mol$_{Al_2O_3}$
Boiling heat	70 kcal/mol$_{Al}$	444 kcal/mol$_{Al_2O_3}$
Volatilization heat	——	444 kcal/mol$_{Al_2O_3}$

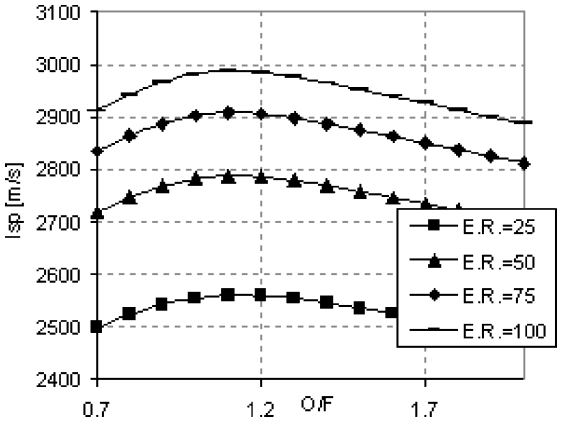

Fig. 1 $I_{sp_{VAC}}$ **vs** O/F **for Al–H_2O system at** $P = 1$ **atm.**

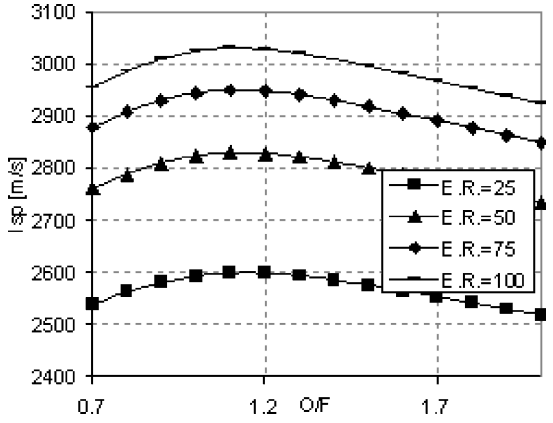

Fig. 2 $I_{sp_{VAC}}$ **vs** O/F **for Al–H_2O system at** $P = 5$ **atm.**

thruster this strategy would complicate matters, requiring a pressurized O_2 tank or pumping. Simplicity and reliability being among the most important satellite (micro)propulsion requirements, this option was not examined further.

Ideal Aluminum–Water Rocket Performance

The purpose of this section is to assess the ideal performance potential of pure Al/steam combinations in terms of adiabatic flame temperature, combustion products, specific impulse in vacuo, and thrust coefficient. The option of adding H_2O_2 to Al and steam was also analyzed. Rocket performance was calculated using NASA's CEA600 equilibrium code.[11] Although its assumptions are highly idealized, they provide a good initial yardstick to preliminarily gauge potential rocket propellants candidates. Assuming initial reactant temperature 300 K, results indicate a specific vacuum impulse $I_{sp_{vac}}$ of order 3000 m/s over a wide range of pressures, oxidizer-to-fuel-weight ratios O/F, and expansion ratios (ER). The dependence of $I_{sp_{vac}}$ on pressure and O/F is mild; the main performance parameter is ER (Figs. 1–5).

High equilibrium temperatures (Fig. 6) also explain the high concentrations of atomic H (Figs. 7 and 8). In Figs. 7 and 8, going from

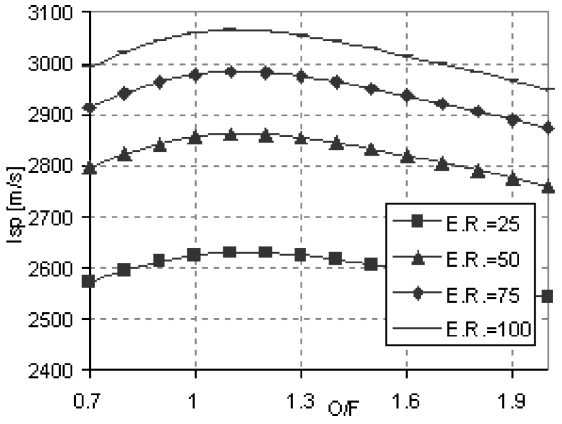

Fig. 3 $I_{sp_{VAC}}$ **vs** O/F **for Al–H_2O system at** $P = 10$ **atm.**

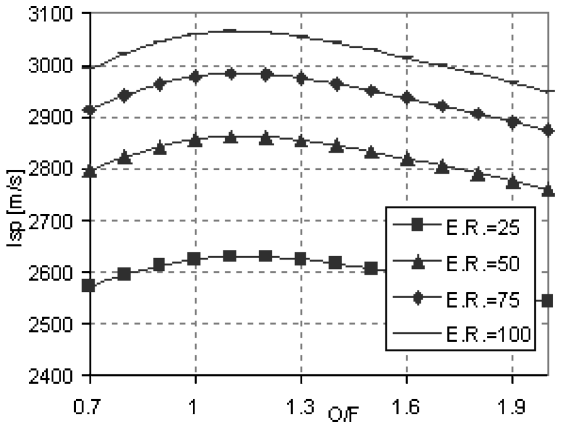

Fig. 4 $I_{sp_{VAC}}$ **vs** O/F **for Al–H_2O system at** $P = 20$ **atm.**

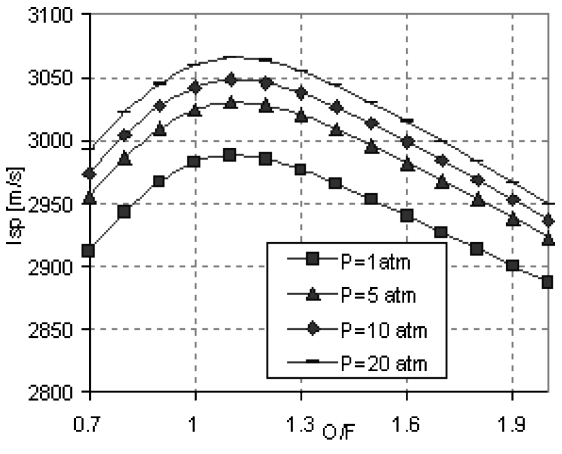

Fig. 5 $I_{sp_{VAC}}$ **vs** O/F **for Al–H_2O system (ER = 100).**

left to right, pressure and equivalence ratio grow respectively from 1 to 20 atm and from 0.4 to 8. These temperatures are in the same range as those predicted in Ref. 6 for Al/O_2 combustion, that is, those of Al_2O_3 volatilization (3450–4000 K), corresponding to the flame temperature if Al vapor reacts with O_2. Actually, for Al_2O_3-coated Al, the flame temperature will be lower, but the CEA600 code cannot account for the heat to bring Al_2O_3 above its boiling point. Because the ΔH_R of the Al/H_2O reaction (~ -230 kcal/mol) is insufficient to vaporize the oxide, the combustion temperature has the oxide boiling temperature as ceiling. In fact, vaporizing the coated metal particle would include about 38.3 kcal/mol$_{Al_2O_3}$ (at $P = 1$ atm) to heat Al_2O_3 to its melting temperature (2370 K), $\sim$28.3 kcal/mol$_{Al_2O_3}$ to melt it, and $\sim$17.9 kcal/molAl_2O_3 to heat it to its boiling point (3273 K). Extra heat will also be required to vaporize water, that

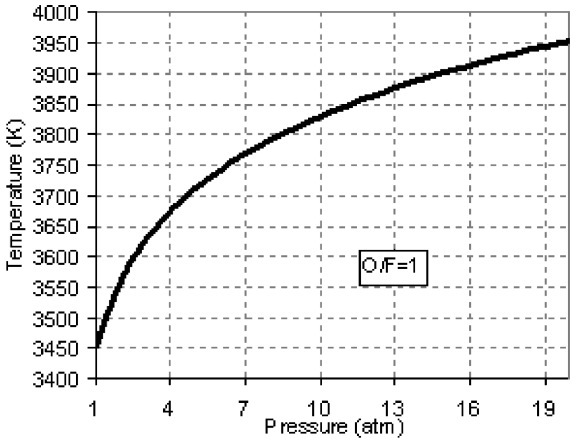

Fig. 6 Temperature vs pressure for Al–H_2O system ($O/F = 1$).

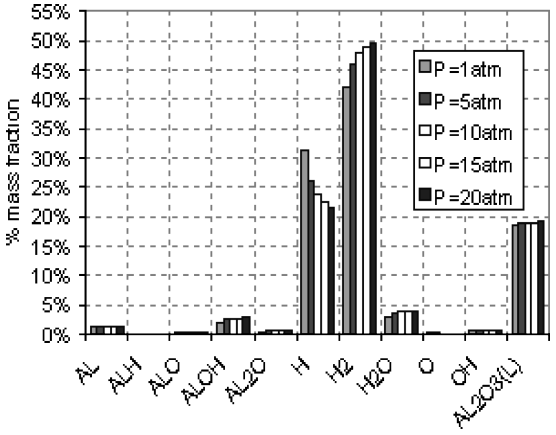

Fig. 7 Species mole fraction (%) for Al–H_2O system ($O/F = 1$).

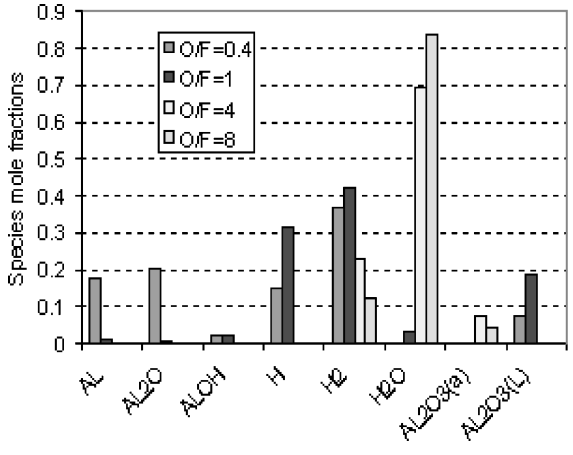

Fig. 8 Species for Al–H_2O system ($P = 1$ atm, ER = 100).

is, ~0.557 kcal/mol_{H_2O} (corresponding to 0.1 kcal/$mol_{Al_2O_3}$) to heat it to its boiling point and 9.71 kcal/mol_{H_2O} (1.74 kcal/$mol_{Al_2O_3}$) to boil it. The heat available to vaporize the oxide is the difference between the heat released by combustion (−230 kcal/mol) and that necessary to heat and boil the reactants (88.47 kcal/molAl_2O_3). Because the oxide heat of vaporization (444 kcal/molAl_2O_3) is larger, the flame temperature will reach up to and stay at the oxide boiling temperature.

These temperatures may pose severe material problems in practical operation unless the equivalence ratio is reduced (O/F increased), the adiabatic flame temperature dropping due to the effect of excess water and of the heat absorbed by the endothermic reaction $H_2 \rightarrow 2H$.

Lower temperatures are beneficial to materials strength, but below the boiling temperature of Al, chemical reactions will occur on its surface, not in the gas phase, and kinetics may be slow. Thus, in order to ensure that Al and water react in the gas phase, the O/F should not be too large; that is, temperatures should be above the Al boiling point (besides, too low temperatures also lower I_{sp} and density I_{sp}). Reasonably high temperatures help in keeping a flame anchored in microrocket chambers,[12] where combustion is less stable because of inherently larger heat losses due to the high surface/volume ratio. The effect of varying the mixture ratio O/F is shown in Figs. 8–10 for conditions representative of some microrocket applications ($P = 1$ atm, ER = 100).

Figure 8 shows that, at lean equivalence ratios, the principal products of Al–water combustion are condensed Al_2O_3 and H_2. Increasing O/F from 0.4 to 1 leads to complete Al conversion and formation of Al_2O_3(L). Because its concentration is high, two-phase-flow losses and severe hardware problems should be expected. These problems could be overcome by properly choosing O/F. Figures 8 and 9 show that the temperature of the products is the result of competition among the heat released by exothermic reactions forming Al_2O_3(L), the heat absorbed by the endothermic reaction $H_2 \rightarrow 2H$, and the presence of excess water. Figure 10 shows that choosing $O/F \sim 4.4$ yields an $I_{sp_{vac}}$ of about 2600 m/s with moderate temperatures (≅2400 K) but slower heterogeneous kinetics. When O/F is reduced to 3, flame temperature rises to 2800 K, higher than the boiling temperature of Al, so that kinetics may become homogeneous. $I_{sp_{vac}}$ is about 2750 m/s.

"Frozen" performance is shown in Figs. 11 and 12 in a restricted range of O/F (5.2–7); outside this range the temperature is lower

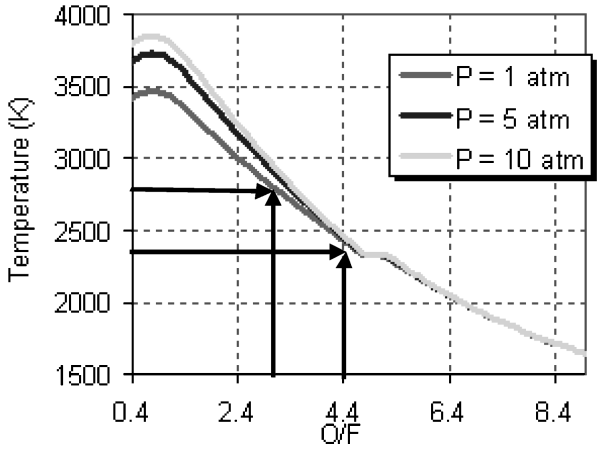

Fig. 9 Temperature vs O/F for Al–H_2O system (ER = 100).

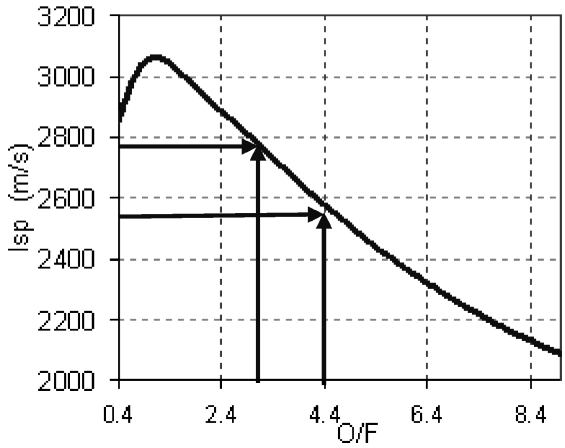

Fig. 10 I_{sp} vs O/F for Al–H_2O ($P = 1$ atm, ER = 100).

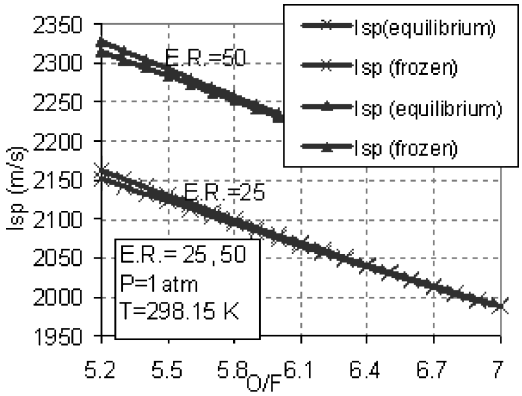

Fig. 11 $I_{sp_{vac}}$ **vs** O/F **(frozen and equilibrium performance).**

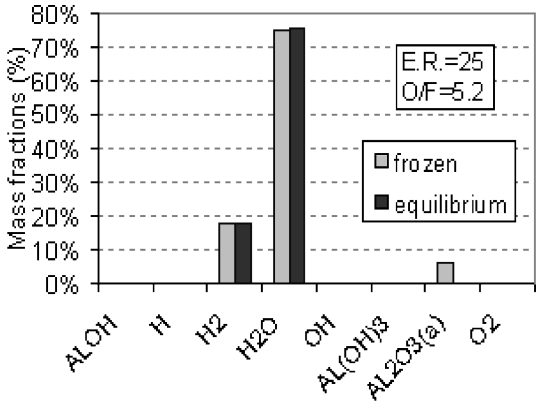

Fig. 12 Species mole fractions (frozen and equilibrium performance).

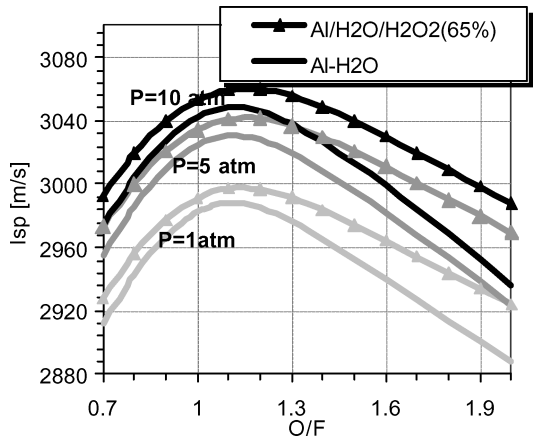

Fig. 13 I_{sp} **trend with Al/H2O and Al/H2O/H2O2(65%).**

than the condensation temperature for Al_2O_3. Within this range there are no substantial differences between the two cases (equilibrium and frozen).

The effect of adding hydrogen peroxide to water was also briefly investigated. Figure 13 shows that 65% H_2O_2–35% water (i.e., commercially available peroxide) raises I_{sp} over a broad range of $O/F \geq 1.1$ and with pressure; at $P = 10$ atm I_{sp} is ~3000 m/s (with ER = 100). For both (Al/H_2O and $Al/H_2O/H_2O_2$(65%), the ideal thrust coefficient C_F stays constant with O/F and equal to 1.74 for all values of O/F examined. Figure 14 compares mole fractions at the combustor exit; even though adding hydrogen peroxide increases the average molar weight from 20.8 to 21.3, $I_{sp_{vac}}$ increases because the combustor temperature increases from 3140.46 to 3283.47 K.

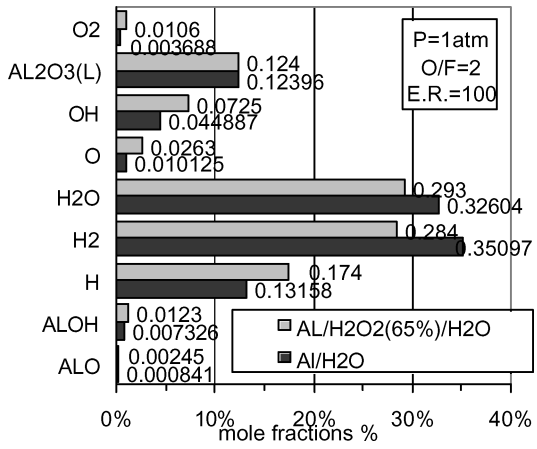

Fig. 14 Species mole fractions at $P = 1$ atm, $O/F = 2$, ER = 100.

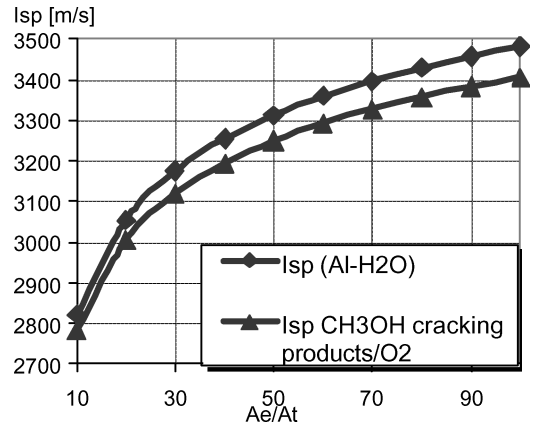

Fig. 15 Comparison of $I_{sp_{vac}}$ **vs Ae/At burning Al/H_2O and CH_3OH cracking productss with O_2.**

From a practical viewpoint, however, commercial-strength hydrogen peroxide could pose safety and storage problems compared to water and complicates a microrocket engine. If simplicity and thrust are preferred to higher specific impulse, water looks to be a better oxidizer.

Figure 15 compares the specific impulse obtained by Al/H_2O combustion to the ideal performance of a methanol–oxygen microrocket, where methanol (CH_3OH) is cracked prior to being burned with oxygen.[13]

At $P = 1$ atm, $O/F = 1$, and 10-to-100 area expansion ratio, Al–water has a 3% higher $I_{sp_{vac}}$ with respect to methanol/oxygen and without the problems posed by O_2 storage in space. So the density I_{sp} reached by the Al–water combination makes it potentially attractive. Further, the Al/H_2O specific impulse (up to ~350 s) compares favorably with that obtained by current hydrazine microrockets (~220 s) and hybrid microrockets (~270 s) (Ref. 14). A further advantage is that storing liquid water is feasible in a broad range of temperatures and pressures, ensuring lighter and more compact propulsion and tankage systems.

Burning Aluminum Particles with Steam: Heating Times

The ideal Al and steam thermodynamic performance shown in the preceding section is interesting enough to followup on with an evaluation of Al particle heating and of oxidation kinetics. Because commercially available Al is covered by an Al_2O_3 layer, this section analyzes heating and melting times of a single particle of Al coated by a layer of Al_2O_3. In fact, no reactions are assumed to occur before Al_2O_3 melts. Heating and melting times contribute to the overall combustion time of a particle and have an impact on flame anchoring, and so they must be estimated.

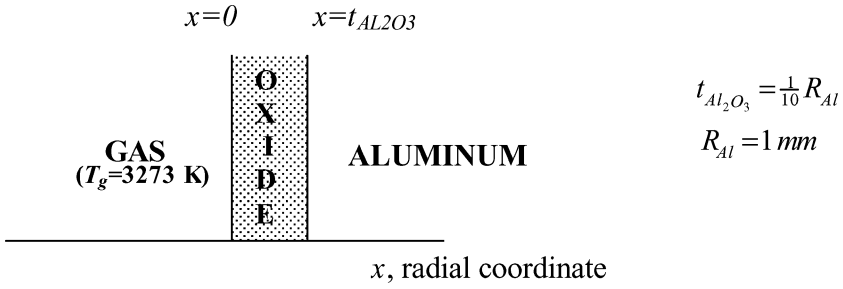

Fig. 16 Geometry of the heating model.

The heating model assumes that $P = 1$ atm and $O/F = 1$; the adiabatic flame temperature for pure Al and water, calculated in the preceding section, is ~3450 K (see Fig. 7). However, because the adiabatic flame temperature cannot be higher than the Al_2O_3 boiling temperature, we assumed this same temperature (~3272 K) for the hot gas surrounding the metal particle. In this environment, the Al_2O_3 coating must be heated from 300 to 1700 K, at which it melts; once it is completely melted, the temperature starts to increase again up to the Al_2O_3 boiling point. For simplicity, in estimating the Al_2O_3 and Al heating, it was assumed that the Al core begins to heat after the Al_2O_3 melts and that, once the Al core reaches its melting point at 933 K, Al_2O_3 begins heating up to its boiling point. Then Al again starts heating up to 2792 K and boils. This is a rough assumption, but it provides a faster and conservative estimate of heating times.

The Al_2O_3 melting time was calculated by solving the Fourier equation up to the phase change. Because the oxide thickness $t_{Al_2O_3}$ is 1/10 of the Al radius ($R_{Al} \sim 1$ mm), a one-dimensional planar analysis is convenient, again providing a conservative time estimate. The geometry is shown in Fig. 16.

The governing equations consist of the energy equations for the solid and liquid Al regions and the momentum and mass conservation equations for the liquid.

The Fourier equation in the solid (subscript s) is

$$\frac{\partial T_s}{\partial \tau} = \alpha_s \frac{\partial^2 T_s}{\partial x^2} \tag{4}$$

where $\alpha_s = k_s/\rho_s c_s$. Assuming no mass forces and zero bulk viscosity, the mass, momentum, and energy equations in the liquid (subscript l) are

$$\frac{\partial v}{\partial x} = 0 \tag{5}$$

$$\rho_l \left(\frac{\partial v}{\partial \tau} + v \frac{\partial v}{\partial x} \right) = -\frac{\partial p}{\partial x} + \mu_l \frac{\partial^2 v}{\partial x^2} \tag{6}$$

$$\frac{\partial T_l}{\partial \tau} + v \frac{\partial T_l}{\partial x} = \alpha_l \frac{\partial^2 T_l}{\partial x^2} \tag{7}$$

where $\alpha_1 = k_1/\rho_1 c_1$, v is the particle velocity, and α, k, ρ, and c are, respectively, thermodiffusivity, thermal conductivity, density, and specific heat.

During the melting process, the liquid/solid interface moves; thus the boundary conditions (BCs) are time dependent. Furthermore, the two phases have different thermophysical properties. To avoid solving for momentum and mass equations, it was assumed that 1) the change of volume on solidification can be neglected, so that the density is the same in both solid and liquid phases, $\rho_l = \rho_s$, and 2) the liquid is quiescent ($v = 0$), so that heat transfer is due only to conduction.

At the interface $X(t)$, between the liquid and solid phases, boundary conditions (8) and (9) are as follows:

$$T_s = T_l = Tm \tag{8}$$

when $x = X(t)$ (the subscript m refers to the melting conditions). The second boundary condition concerns the absorption of latent heat, L, at this surface. In fact, the heat supplied by conduction is equal to the heat $L_\rho \, dX$ absorbed per unit area, when the separation surface moves by a distance dX; that is,

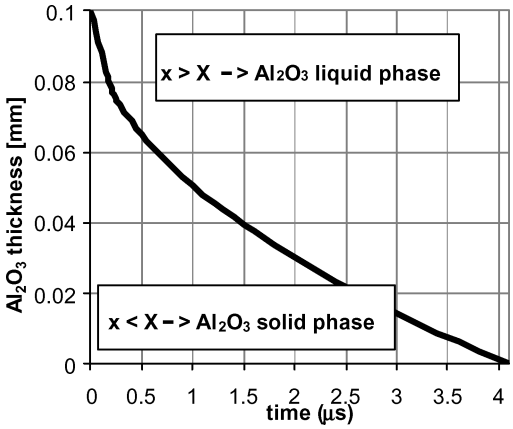

Fig. 17 Alumina separation surface X history ($R_{Al} = 1$ mm).

$$k_l \frac{\partial T_l}{\partial x} - k_s \frac{\partial T_s}{\partial x} = L\rho \frac{dX}{d\tau} \tag{9}$$

To solve Eqs. (6–9), additional boundary conditions have to be provided. In particular, the Al_2O_3 boundary conditions are

$$T_s^{Al_2O_3} = T_0^{Al_2O_3} = 300 \text{ K}, \qquad \tau = 0, x > 0 \tag{10}$$

$$T_l^{Al_2O_3} = T_b^{Al_2O_3} = T_g = 3273 \text{ K}, \qquad x = 0, \tau > 0 \tag{11}$$

This means that in the region $0 < x < \tau Al_2O_3$ is initially solid at $T_s = 300$ K; the surface $x = 0$ (the separation surface between the oxide and the hot gas) is maintained at constant temperature $T_g = 3273$ K, above the the Al_2O_3 melting point (~1700 K). The subscript 0 indicates the initial condition at $\tau = 0$; g refers to the gas phase and b to the boiling condition the solution of Eqs. (4–7) (see the Appendix) is

$$T_s = T_0 + \frac{T_m - T_0}{\text{erfc}\left[\lambda\sqrt{(\alpha_l/\alpha_s)}\right]} \text{erfc} \frac{x}{2\sqrt{\alpha_s \tau}} \tag{12}$$

$$T_l = T_g - \frac{(T_g - T_m)}{\text{erf}\lambda} \text{erf} \frac{x}{2\sqrt{\alpha_l \tau}} \tag{13}$$

with the constant $\lambda \cong -1$.

For the condition investigated ($P = 1$ atm, $O/F = 1$, $R_{Al} = 1$ mm, $t_{Al_2O_3} = 0.1$ mm), Fig. 17 shows that the time required to melt the Al_2O_3 is about 4.2 μs.

Figure 18 shows Al_2O_3 heating times of order 0.042 ps. Once Al melts, ignition of the Al surface may take place. However, for fast kinetics, reactions should occur in the gas phase: thus, the time required to heat the whole metal particle up to its boiling point was calculated by estimating Al heating, melting, and boiling times and adding them to the time to heat Al_2O_3 up to its boiling point. Al core heating and melting times were calculated using the same

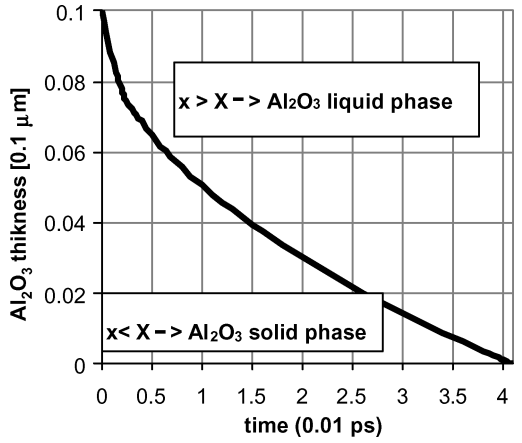

Fig. 18 Alumina separation surface X history ($R_{Al} = 0.1$ μm).

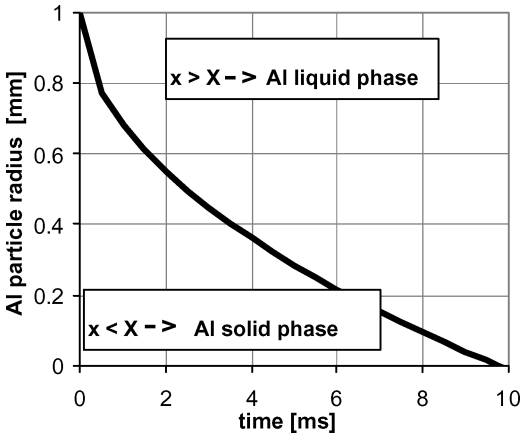

Fig. 19 Aluminum separation surface X history ($R_{Al} = 1$ mm).

equations reported in the Appendix. To simplify calculations, Al particles were assumed to heat and melt after the oxide reaches its melting temperature. Although conservative, this assumption makes it possible to estimate heating and melting times quickly. The Al boundary conditions are

$$T_s^{Al} = T_0^{Al} = 300K, \qquad \tau = 0, \qquad x > 0 \tag{14}$$

$$T_l^{Al} = T_m^{Al_2O_3} = 1700K, \qquad x = 0, \qquad \tau > 0 \tag{15}$$

where now $x = 0$ corresponds to the separation surface between the Al solid core and its liquid oxide. The solution for the Al temperature (Fig. 19) shows an Al melting time of about 9.8 ms; that is, under these conservative assumptions, heating of the particle is essentially controlled by Al heating.

The same analysis was performed assuming a nanoparticle of radius 0.1 μm. Figure 20 shows that the time required to melt the Al particle completely is about 0.098 μs. Thus the Al_2O_3 heating time (0.042 ps) is negligible compared to that of Al: the total time needed to heat and melt the particle ($R_{Al} = 0.1$ μm) is ~0.098 μs.

Based on these times, the heat necessary to raise the temperature of the Al_2O_3 coating (for an Al particle of radius 1 mm) up to its boiling point is about 1600 kJ/kg; the corresponding thermodiffusion time is $t_{diff}^{Al_2O_3} = t_{Al_2O_3}^2/\alpha_l^{Al_2O_3} = 16.4$ μs. To heat Al from melting to boiling, about 2137 kJ/kg is needed. The time estimated is $t_{diff}^{Al} = R_{Al}^2/\alpha_l^{Al} = 0.0317$ s. For a 0.1-μm-radius particle, the same estimates obtain: $t_{diff}^{Al_2O_3} = 0.164$ ps, $t_{diff}^{Al} = 317$ ps. These results are summarized in Table 2, showing very rapid heating and suggesting that ignition could be controlled by Al–steam kinetics.

Table 2 Al heating times for 1-mm and 0.1-μm l particles

	Al particle radius: 1 mm		Al particle radius: 0.1 μm	
Parameter	Al core	Al layer	Al core	Al layer
Heating up to melting temperature	9.8 ms	4.2μs	98ps	0.042 ps
Heating up to boiling temperature	0.0317 s	16.4μs	317 ps	0.164 ps
Total heating time	0.0415 s	20.6μs	415 ps	20.6 ps

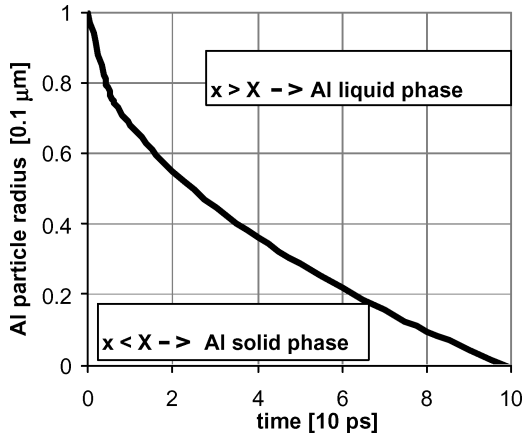

Fig. 20 Aluminum separation surface X history ($R_{Al} = 0.1$ μm).

Kinetics and Ignition

Al ignition data are scarce, so the present calculations were restricted to gas-phase reactions only by separating the ignition reactions that form AlO and AlO_2 (only mildly exothermic) from the much faster and more exothermic heterogeneous condensation and completion reactions that form Al_2O_3. Detailed ignition of a single Al nanoparticle will be investigated in a separate study now under way. Al–steam mixtures were therefore assumed to be preheated at $T = 3273$ K, that is, higher than the Al_2O_3 melting and boiling points. Gas-phase kinetics was simulated using rates k_3–k_6 in Refs. 15–17. A detailed kinetic scheme is as follows:

Surface reactions:

$$Al_{(l)} \rightarrow Al_{(g)} \tag{R1}$$

$$Al_{(l)} + AlO_{(g)} \rightarrow Al_2O_{(g)} \tag{R2}$$

Gas phase reactions:

$$Al_{(g)} + O_2 \rightarrow AlO + O$$

$$k_3 = 9.76 \times 10^7 \exp(-80/T)\mathrm{m^3 mol^{-1} s^{-1}} \tag{R3}$$

$$AlO + O_2 \rightarrow AlO_2 + O$$

$$k_4 = 4.63 \times 10^8 \exp(-10{,}008/T) \tag{R4}$$

$$Al + H_2O \rightarrow AlO + H_2$$

$$k_5 = (1.9 \pm 1.5) \times 10^4 \exp[-(442.87 \pm 221.44)/T] + (1.6 \pm 0.7) \times 10^2 \exp[-(2868.6 \pm 452.94)/T] \tag{R5}$$

$$O + O + M \rightarrow O_2 + M, \qquad k_6 = 6.17 \times 10^7 \times T^{-0.5} \tag{R6}$$

Dissociation reaction:

$$Al_2O_{3(l)} \rightarrow 2AlO + 1/2\,O_2 \tag{R7}$$

Condensation reactions:

$$2AlO + 1/2\,O_2 \rightarrow Al_2O_{3(l)} \tag{R8}$$

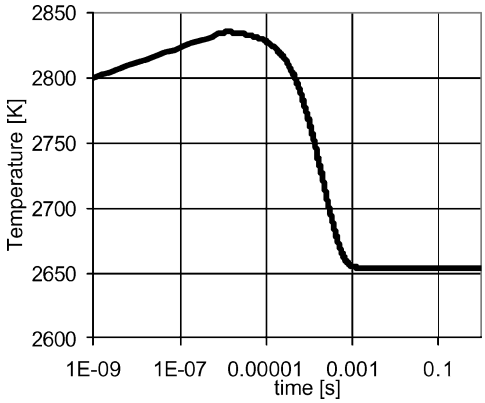

Fig. 21 Temperature vs time for Al–H_2O system ($O/F = 1$, $P = 1$ atm).

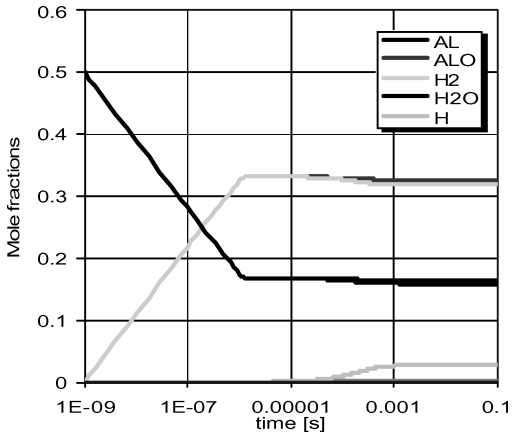

Fig. 22 Species mole fractions for Al–H_2O ($O/F = 1$, $P = 1$ atm), R3–R6 only.

$$2AlO + H_2O \rightarrow Al_2O_{3(l)} + H_2 \quad \text{(R9)}$$

$$Al_2O + O_2 \rightarrow Al_2O_{3(l)} \quad \text{(R10)}$$

$$Al_2O + 2H_2O \rightarrow Al_2O_{3(l)} + 2H_2 \quad \text{(R11)}$$

$$AlO_2 + AlO_2 \rightarrow Al_2O_{3(l)} + 1/2\,O_2 \quad \text{(R12)}$$

Reaction rate (R5) indicates that Al and steam combustion follows two reaction paths, the first dominating at low temperatures, the second at high temperatures.[17] Kinetic calculations are performed at high temperatures, and so only the second path was considered.

Figure 21 shows that after 10 μs the temperature decreases from 2800 K (initial) to ~2660 K due to the rapid endothermic formation of H atoms (Fig. 22). Comparing these times to those associated with heating, the conclusion is that Al/steam combustion will indeed be controlled by kinetics or, possibly, by mixing. Even so, the present simulations predict ignition delays of order 10^{-5} s at pressure 1 atm.

Flame Anchoring in Microrockets

In typical turbulent flames ($Re \sim 10^5$–10^7), kinetic times of order 0.1 ms or shorter are a sign of stable flame anchoring. For microrocket applications, however, this estimate must be consistent with the physical size of the device. Assuming conservatively a scale of 1 cm and a rocket pressure of 20 atm, the Reynolds number could reach 10^5 to 10^6, and the Kolmogorov scale 10^{-3} to 10^{-4} cm. Turbulent (mixing) times ($\sim k/e$) in this range of Reynolds numbers, using the Taylor scale for reference, are therefore of order 0.1–0.01 ms, that is, of the same order of kinetics (though calculated at much lower pressure). Although these are crude estimates, they point to a possible distributed combustion regime rather than to the "thin flame" or flamelet regime more common in propulsion applications. Distributed combustion may work just as efficiently, provided that the reactants plus products are brought quickly to sufficiently high temperature by mixing.[18] Recycling wall-heat losses to vaporize water may indeed obtain this goal. In any event, this analysis suggests that Al–water flame anchoring in microrockets should be further investigated.

Conclusions

In the first part of this paper we briefly analyzed the equilibrium performance (specific impulse, equilibrium temperature, and composition in the combustion chamber) of Al and steam. Performance of Al with H_2O looks very promising for satellite/microrocket propulsion. Operating at equivalence ratio $O/F \sim 3$ leads to temperature ~2800 K and interesting specific impulse (~3000 m/s). These temperatures are high but not forbidding and are beneficial in keeping a flame anchored in microrocket chambers; wall heat losses due to high chamber temperatures might be compensated by use to regeneratively vaporize water before it enters the microcombustion chamber. This scheme is more complex but is also more efficient. Simplified calculations show that small particles (1 mm and below) ensure heating times on the order of 415 ps and a mixing time of 10 μs with a total heating and ignition delay time of about 10 μs, account being made for the presence of an Al_2O_3 coat. Under these conditions Al–H_2O combustion looks like a remarkable alternative to conventional propellant. The nontrivial question of how the motor can be started will likely be answered by burning pure Al, that is, before its Al_2O_3 coating may have time to form.

Appendix: Solution of Heating Equations

The general solution of Eqs. (4) and (7) is

$$T_s = T_0 + A\,\mathrm{erfc}\left(x \Big/ 2\sqrt{\alpha, \tau}\right) \quad \text{(A1)}$$

$$T_l = T_g - B\,\mathrm{erf}\left(x \Big/ 2\sqrt{\alpha, \tau}\right) \quad \text{(A2)}$$

where A is a constant that satisfies boundary conditions (10) and (4):

$$\frac{\partial^2 T_s}{\partial x^2} = \frac{1}{\alpha_s}\frac{\partial T_s}{\partial \tau} = \frac{Axe^{x^2/4\alpha_s\tau}}{2\sqrt{\pi}(\alpha_s\tau)^{\frac{3}{2}}}$$

and B is a constant that satisfies boundary conditions (11) and (7):

$$\frac{\partial^2 T_l}{\partial x^2} = \frac{1}{\alpha_l}\frac{\partial T_l}{\partial \tau} = \frac{Bxe^{x^2/4\alpha_l\tau}}{2\sqrt{\pi}(\alpha_l\tau)^{\frac{3}{2}}}$$

By replacing Eq. (8) with Eqs. (1a) and (2a) an equation for $X(\tau)$ is obtained:

$$T_0 + A\mathrm{erfc}\frac{X}{\sqrt[2]{\alpha_s\tau}} = T_g - B\mathrm{erf}\frac{X}{2\sqrt{\alpha_l\tau}} = T_m \quad \text{(A3)}$$

Because Eq. (A3) has to be satisfied at all times, X must be proportional to $\tau^{1/2}$; that is,

$$X = 2\lambda\sqrt{\alpha_s\tau} \quad \text{(A4)}$$

where λ is a numerical constant to be found from Eq. (9).

The constants A and B are calculated using Eqs. (A3) and (A4):

$$A = \frac{T_m - T_0}{\mathrm{erfc}\left[\lambda\sqrt{(\alpha_l/\alpha_s)}\right]}$$

and

$$B = (T_g - T_m)/\mathrm{erf}\lambda$$

thus

$$T_s = T_0 + \frac{T_m - T_0}{\mathrm{erfc}\left[\lambda\sqrt{(\alpha_l/\alpha_s)}\right]}\mathrm{erfc}\frac{x}{2\sqrt{\alpha_s\tau}} \quad \text{(A5)}$$

$$T_l = T_g - \frac{(T_g - T_m)}{\mathrm{erfc}\lambda}\mathrm{erfc}\frac{x}{2\sqrt{\alpha_s\tau}} \quad \text{(A6)}$$

where the constant λ is the solution of the equation

$$\frac{e^{-\lambda^2}}{\mathrm{erf}\lambda} - \frac{k_s}{k_l}\sqrt{\frac{\alpha_l}{\alpha_s}}\frac{T_m - T_0}{T_g - T_m}\frac{e^{-(\alpha_l/\alpha_s)\lambda^2}}{\mathrm{erfc}\left[\lambda\sqrt{\alpha_l/\alpha_s}\right]} = \frac{\lambda L\sqrt{\pi}}{c_l(T_g - T_m)} \quad \text{(A7)}$$

obtained using Eqs. (9), (A4), (A5), and (A6). Equation (A7) was solved by the Newton–Raphson method, and λ was found to be $\cong -1$.

References

[1]Bruno, C., Ingenito, A., and Cuoco, F., "Using Powdered Aluminum for Space Propulsion," *Proceedings of the 18th International Workshop on Rocket Propulsion: Present and Future*, Pozzuoli, 16–20 June 2002.

[2]Foote, J. P., Thompson, B. R., and Lineberry, J. T., "Combustion of Aluminum with Steam for Underwater Propulsion," *Advances in Chemical Propulsion*, edited by G. Roy, CRC Press, Boca Raton, FL, 2002, Chap. 8, pp. 133–146.

[3]Greiner, L., "Selection of High Performing Propellants for Torpedoes," *ARS Journal*, Vol. 30, Dec. 1960, pp. 1161–1163.

[4]Tepper, F., and Kaledin, L. A., "Combustion Characteristics of Kerosene Containing ALEX^{TM} NANO-ALUMINUM," *Combustion of Energetic Materials*, edited by K. Kuo, and L. De Luca, Begell House Press, New York, 2002, pp. 195–205.

[5]Friedman, R., and Macek, A., "Ignition and Combustion of Aluminum Particles in Hot Ambient Gasses," *Combustion and Flame*, Vol. 6, No. 1, 1962, pp. 9–19.

[6]Glassman, I., "Metal Combustion Thermodynamics," *Combustion*, 3rd ed., Academic Press, San Diego, CA, 1977, Chap. 9, pp. 436–457.

[7]Price, E. W., "Combustion of Metalized Propellants," *Fundamentals of Solid Propellant Combustion*, Progress in Astronautics and Aeronautics, Vol. 90, AIAA, New York, 1983, Chap. 9, pp. 479–513.

[8]Merzhanov, A. G., Grigorjev, Y. M., and Gal'chenko, Y. A., "Aluminum Ignition," *Combustion and Flame*, Vol. 29, No. 1, 1977, pp. 1–14.

[9]Kuehl, D. K., "Ignition and Combustion of Aluminum and Beryllium," *AIAA Journal*, Vol. 3, No. 12, 1965, pp. 2239–2247.

[10]Widener, J. F., Liang, Y., and Beckstead, M. W., "Aluminum Combustion Modeling in Solid Propellant Enviroments," AIAA Paper 99-0449, Dec. 1999.

[11]Gordon, S., and McBride, B. J., "Computer Program for Calculation of Complex Chemical Equilibrium Compositions and Applications, Part II. Users Manual and Program Description," NASA Ref. Pub. 1311, June 1996.

[12]Bruno, C., "Chemical Microthrusters: Effect of Scaling on Combustion," AIAA Paper 2001-3711, July 2001.

[13]Bruno, C., Giacomazzi, E., and Ingenito, A., "Pyrolysis of Methanol for Microrocket Applications," *Proceedings of the AIDAA XVII National Congress*, edited by M. Marchetti, ESAGRAFICA Press, Rome, 2003.

[14]Maisonneuve, Y., Godon, J. C., Lecourt, R., Lengelle, G., and Pillet, N., "Hybrid Propulsion for Small Satellites Design Logic and Tests," *Combustion of Energetic Materials*, edited by K. Kuo, and L. De Luca, Begell House Press, New York, 2002, pp. 90–100.

[15]Brooks, K. P., and Beckstead, M. W., "Dynamics of Aluminum Combustion," *Journal of Propulsion and Power*, Vol. 11, No. 4, 1995, pp. 769–780.

[16]Liang, Y., Beckstead, M. W., and Pudduppakkam, K. V., "Numerical Simulation of Unsteady, Single Aluminum Particle Combustion," *36th JANNAF Combustion Meeting*, Chemical Propulsion Information Agency 691, Coca Beach, FL, Vol. 1, Oct. 1999, pp. 283–309.

[17]Servaites, J., Krier, H., Melcher, J. C., and Burton, R. L., "Ignition and Combustion of Aluminum Particles in Shocked H_2O/O_2/Ar and CO_2/O_2/Ar Mixtures," *Combustion and Flame*, Vol. 125, Nos. 1–2, 2001, pp. 1040–1054.

[18]Tabacco, D., Innarella, C., and Bruno, C., "Theoretical and Numerical Investigation on Flameless Oxidation," *Combustion Science and Technology*, Vol. 174, No. 7, 2002, pp. 1–35.